**Cell Reports, Volume *22***

## Supplemental Information

# Cell-Type Specificity of Callosally Evoked Excitation and Feedforward Inhibition in the Prefrontal Cortex

**Paul G. Anastasiades, Joseph J. Marlin, and Adam G. Carter**

## SUPPLEMENTAL EXPERIMENTAL PROCEDURES

### Animals

Experiments used wild-type, heterozygous PV-Cre (Hippenmeyer et al., 2005), heterozygous SOM-Cre (Taniguchi et al., 2011), or PV- and SOM-Cre crossed with homozygous Ai14 tdTomato Cre-reporter line (Madisen et al., 2010) mice of either sex in a C57BL/6J background (all mice purchased from Jackson laboratories). Data were collected from166 mice, with recordings from 125 pairs of neurons and an additional 140 single cells. All experimental procedures were approved by the University Animal Welfare Committee of New York University.

### Stereotaxic injections

Mice aged 4-6 weeks were deeply anesthetized with a mixture of ketamine (10 mg/mL) and xylazine (0.1 mg/mL), and head-fixed in a stereotax (Kopf Instruments). A small craniotomy was made over the injection site, using coordinates relative to Bregma: prelimbic PFC = −2.1, ±0.4, +2.2 mm; mediodorsal thalamus (MD) = -3.6, -0.3, -0.5 mm (dorsoventral, mediolateral, and rostrocaudal axes). For retrograde labeling, pipettes were filled with either red or green retrobeads (Lumafluor) or Cholera Toxin Subunit B (CTB) conjugated to either Alexa 488, 555 or 647 (Life Technologies). Viruses varied between experiment and included: AAV1-hSyn-hChR2(H134R)-EYFP (UPenn, $9.32x10^{12}$ GC/mL) for long-range excitatory inputs; AAV1-EF1a-DIO-hChR2(H134R)-EYFP (UPenn, $1.93x10^{13}$ GC/mL) for local inhibitory inputs; and AAV1-CAG-FLEX-tdTomato (UPenn, $7.88x10^{12}$ GC/mL) or AAV1-CAG-FLEX-EGFP (UPenn, $9.16x10^{12}$ GC/mL) for labeling of interneurons in either PV- or SOM-Cre mice. To study cPFC inputs at retrogradely labeled neurons, virus was mixed with retrobeads or CTB in a 1:1 ratio. Borosilicate pipettes with 5–10 μm tip diameters were back-filled, and 130-550 nL was pressure injected using a Nanoject II (Drummond), with 30 s between injections. The pipette was subsequently left in place for an additional 5 min, allowing time to diffuse away from the tip, before being slowly retracted from the brain. Animals were returned to their cages for between 1-3 weeks before recording.

**Slice preparation**

Mice aged 6-8 weeks of either sex were anesthetized with a lethal dose of ketamine (25 mg/mL) and xylazine (0.25 mg/mL), and perfused intracardially with ice-cold external solution containing the following (in mM): 65 sucrose, 76 NaCl, 25 $NaHCO_3$, 1.4 $NaH_2PO_4$, 25 glucose, 2.5 KCl, 7 $MgCl_2$, 0.4 Na-ascorbate, and 2 Na-pyruvate (295–305 mOsm), and bubbled with 95% $O_2$/5% $CO_2$. Coronal slices (300 μm thick) were cut on a VS1200 vibratome (Leica) in ice-cold external solution, before being transferred to ACSF containing the following (in mM): 120 NaCl, 25 $NaHCO_3$, 1.4 $NaH_2PO_4$, 21 glucose, 2.5 KCl, 2 $CaCl_2$, 1 $MgCl_2$, 0.4 Na-ascorbate, and 2 Na-pyruvate (295–305 mOsm), bubbled with 95% $O_2$/5% $CO_2$. Slices were kept for 30 min at 35°C, before being allowed to recover for 30 min at room temperature. All recordings were conducted at 30−32°C.

**Electrophysiology**

Whole-cell recordings were obtained from layer 5 pyramidal neurons located in the prelimbic region of the PFC at a depth of 450–550 μm from the midline. Neurons were identified by infrared-differential interference contrast, as previously described (Chalifoux and Carter, 2010), and projection target was established by the presence of retrobeads or CTB, as previously described (Little and Carter, 2013). Pairs of neighboring neurons were chosen for sequential recording, ensuring they received similar inputs (typically < 50 μm between cells, range 15-130 μm). The order of patching CC and CT neurons was randomized across experiments to avoid any bias. Borosilicate pipettes (2–5 MΩ) were filled with one of two internal solutions. For current-clamp recordings (in mM): 135 K-gluconate, 7 KCl, 10 HEPES, 10 Na-phosphocreatine, 4 $Mg_2$-ATP, 0.4 Na-GTP and 0.5 EGTA, 290–295 mOsm, pH 7.3, with KOH. For voltage-clamp recordings (in mM): 135 Cs-gluconate, 10 HEPES, 10 Na-phosphocreatine, 4 $Mg_2$-ATP, 0.4 Na-GTP, 0.5 EGTA, 10 TEA-chloride, and 2 QX314, 290–295 mOsm, pH 7.3, with CsOH. For some experiments, 30 μM Alexa Fluor 594 was included for morphological reconstructions. For experiments involving 2-photon imaging, fluorescent dye diffused throughout the dendrites for at least 20 min before imaging. Three-dimensional reconstructions of dendritic morphologies were performed using NeuronStudio (Wearne et al., 2005), while two-dimensional tracing of dendrites for figures was performed using Neurolucida (MBF Bioscience).

Electrophysiology recordings were made with a Multiclamp 700B amplifier (Axon Instruments), filtered at 4 kHz for current-clamp and 2 kHz for voltage-clamp, and sampled at 10 kHz. The initial series resistance was <20 MΩ, and recordings were ended if series resistance rose above 25 MΩ. For current-clamp recordings, neurons were held at -75 mV, unless otherwise noted. For voltage-clamp recordings, EPSCs and IPSCs were recorded at -70 mV and +10 mV, respectively. In a subset of experiments, 1 μM TTX was added to block APs, and 100 μM 4-AP and 4 mM external Ca2+ to restore release. In many experiments, 10 μM CPP with 10 μM gabazine were used to isolate AMPA receptors, and 10 μM NBQX with 10 μM CPP were used to isolate GABAa receptors. For current-clamp recordings, 2 μM CGP-55845 was also included to block GABAb receptors. 10 μM ZD-7288 was used in voltage-clamp recordings and in some current-clamp recordings to block h-current. All chemicals were purchased from Sigma or Tocris Bioscience.

**Dynamic-clamp recordings**

Dynamic-clamp recordings were performed using an ITC-18 interface (Heka Electronics) with Igor Pro (Wavemetrics) running MafPC (courtesy of Matthew Xu-Friedman). Experimentally recorded EPSCs and IPSCs (4 ms LED pulse duration) were first converted into excitatory and inhibitory conductances by dividing by the driving force. Conductances were then injected into neurons, with the dynamic-clamp operating at 50 kHz. The reversal potentials for AMPA-R excitation and GABAa-R inhibition were set as +10 mV and -75 mV, respectively. For feed-forward inhibition, the onset delay of the inhibitory conductance was set to 4 ms, based on voltage-clamp experiments. For suprathreshold experiments, both excitatory and inhibitory conductances were multiplied by a range of scale factors (1-10X) to mimic increasing synaptic activity at a fixed excitation / inhibition ratio (McGarry and Carter, 2016).

**Optogenetics**

ChR2 was expressed in presynaptic neurons or axons and activated using a brief pulse (1 to 8 ms) from a blue LED (473 nm) (Thorlabs). Due to variability in ChR2 expression across slices and animals, LED pulse power and duration were adjusted to obtain reliable responses in each slice (typically ~100-500 pA for

voltage clamp experiments and ~5-10 mV for current clamp experiments). Using these stimulation parameters, LED power was ~ 0.4-10 mW at the back aperture of the objective. For experiments using multiple durations, LED power was set to evoke increasing responses across the range of pulse durations. For wide-field illumination, light was transmitted via a 10x 0.3 NA objective (Olympus) centered 350 μm from the midline. For subcellular mapping, a 60x 1.0 NA objective (Olympus) was targeted to the dendrites, with an effective diameter of < 200 μm.

**Two-photon microscopy**

Two-photon imaging was performed on a custom microscope, as previously described (Chalifoux and Carter, 2010). A Ti:Sapphire laser (Coherent) tuned to 810 nm was used to excite Alexa Fluor 594 to image morphology with a 60x 1.0 NA objective (Olympus).

**Histology and fluorescence microscopy**

Mice were anesthetized with a lethal dose of ketamine (25 mg/mL) and xylazine (0.25 mg/mL) and perfused intracardially with 0.01 M phosphate buffered saline (PBS) followed by 4% paraformaldehyde (PFA) in 0.01 M PBS. Brains were fixed in 4% PFA in 0.01 M PBS overnight (for no antibody staining) or for 4-5 hours (for antibody staining) at 4°C. Slices were prepared at 50-70 μm thickness (Leica VT 1000S vibratome). For PV and SOM antibody labelling, slices were washed once in PBS (0.01 M), once in PBS-T (0.2 % Triton-X100), and blocked in PBS-T with 1 % w/v bovine serum albumin (BSA) for one hour, all at room temperature. Primary antibody incubation (mouse anti-parvalbumin, MAB1572, Millipore, 1:2000; rat anti-somatostatin, MAB354, Millipore, 1:400) was performed at 4$^{o}$C overnight. Slices were then washed 4x in PBS at RT before incubating with secondary antibody (goat anti-rat conjugated to Alexa 647, A-21247, Fisher-Invitrogen, 1:200; goat anti-mouse conjugated to Alexa 647, AB150119, Abcam, 1:200) in PBS-T + BSA for 1 hour. Slices were washed a further 3x in PBS before being mounted. All slices were mounted under glass coverslips on gelatin-coated slides using ProLong Gold antifade reagent with DAPI (Invitrogen). Whole-brain images were acquired using a slide-scanning microscope (Olympus VS120) with a 10x 0.25 NA or 20x 0.75 NA objective. Excitation wavelengths were 387, 485, 560 and 650 nm for DAPI, FITC, TRITC and Cy5, respectively. PFC images were acquired using a confocal microscope (Leica

SP8) with 10x 0.4 NA or 20x 0.75 NA objective. Excitation wavelengths were 405, 488, 552 and 638 nm for DAPI, FITC, TRITC and Cy5, respectively. Image processing involved adjusting brightness and contrast using ImageJ (NIH). Cell counting was performed in a 400 x 150 µm region of interest across layer 5 of the prelimbic PFC for CC, CT and PT comparisons, and a 300 x 1000 µm region of interest for interneuron antibody staining experiments.

**Rabies anatomy**

For monosynaptic rabies virus tracing, AAV1-EF1a-FLEX-TVA-Cherry (UNC, $4.00x10^{12}$ GC/mL) was mixed with AAV1-CA-FLEX-RG (UNC, $4.00x10^{12}$ GC/mL) in a 1:1 ratio, and a total volume of 750 nL was injected into a single hemisphere of the PFC of PV-Cre or SOM-Cre mice. After allowing 2 weeks for expression of these helper viruses, 500 nL of SADΔG-GFP(EnvA) rabies virus (Salk, $4.25x10^{8}$ GC/mL) was injected at the same location. After an additional 8-10 days to allow for monosynaptic retrograde labeling, mice were perfused and slices prepared for fluorescent microscopy.

**Data analysis**

Electrophysiology and imaging data were acquired using National Instruments boards and MATLAB (MathWorks). Wave averaging and off-line analysis was performed using Igor Pro (WaveMetrics). Input resistance was measured using the steady-state response to a 500 ms, -50 pA current injection. The membrane time constant (tau) was measured using exponential fits to these same hyperpolarizations. Voltage sag due to h-current was calculated by taking the minimum voltage in the first 200 ms, subtracting the average voltage over the final 100 ms, and dividing by the steady-state value. PSC and PSP amplitudes were measured as the average value across 1 ms around the peak response. PSP decays were calculated using exponential fits from the peak response back to baseline. Summary data are reported in the text and figures as arithmetic mean ± SEM. Input ratios are reported as geometric mean with 95 % confidence intervals (CI). Comparisons between unpaired data were performed using two-tailed Mann-Whitney U tests. Comparisons between data recorded in pairs were performed using two-tailed Wilcoxon matched-pairs signed rank tests. Ratio data were compared to a theoretical median of 1.0 using Wilcoxon signed rank tests. Firing curves were compared using two-way ANOVA analysis with correction for

multiple comparisons. Statistical tests were performed in GraphPad Prism (version 7.0c). All experiments contain data recorded from at least 3 animals. Significance was defined as $p < 0.05$.

**SUPPLEMENTAL REFERENCES**


Chalifoux, J.R., and Carter, A.G. (2010). GABAB receptors modulate NMDA receptor calcium signals in dendritic spines. Neuron 66, 101-113.

Hippenmeyer, S., Vrieseling, E., Sigrist, M., Portmann, T., Laengle, C., Ladle, D.R., and Arber, S. (2005). A developmental switch in the response of DRG neurons to ETS transcription factor signaling. PLoS Biol 3, e159.

Little, J.P., and Carter, A.G. (2013). Synaptic mechanisms underlying strong reciprocal connectivity between the medial prefrontal cortex and basolateral amygdala. J Neurosci 33, 15333-15342.

Madisen, L., Zwingman, T.A., Sunkin, S.M., Oh, S.W., Zariwala, H.A., Gu, H., Ng, L.L., Palmiter, R.D., Hawrylycz, M.J., Jones, A.R.*, et al.* (2010). A robust and high-throughput Cre reporting and characterization system for the whole mouse brain. Nat Neurosci 13, 133-140.

McGarry, L.M., and Carter, A.G. (2016). Inhibitory Gating of Basolateral Amygdala Inputs to the Prefrontal Cortex. J Neurosci 36, 9391-9406.

Taniguchi, H., He, M., Wu, P., Kim, S., Paik, R., Sugino, K., Kvitsiani, D., Fu, Y., Lu, J., Lin, Y.*, et al.* (2011). A resource of Cre driver lines for genetic targeting of GABAergic neurons in cerebral cortex. Neuron 71, 995-1013.

Wearne, S.L., Rodriguez, A., Ehlenberger, D.B., Rocher, A.B., Henderson, S.C., and Hof, P.R. (2005). New techniques for imaging, digitization and analysis of three-dimensional neural morphology on multiple scales. Neuroscience 136, 661-680.

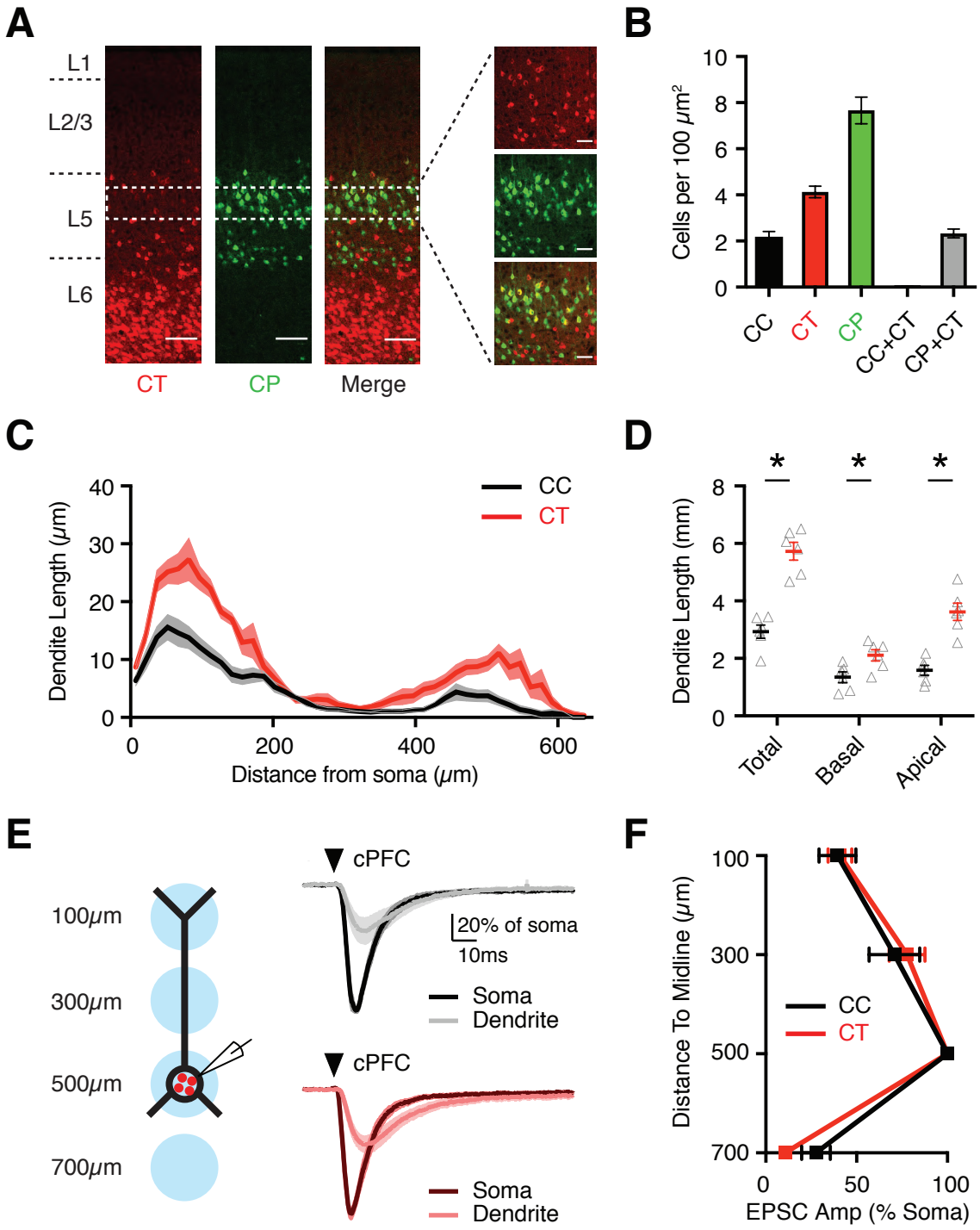


Anastasiades et al., Figure S1

**SUPPLEMENTAL FIGURE LEGENDS**

**Figure S1: Properties of projection neurons and cPFC inputs to their dendrites**

***Related to Figure 1.***

**A)** Confocal images showing the distributions of CT neurons (*left*) and CP neurons (*middle*), along with merged image (*right*) showing co-localization across layers of the prelimbic PFC (scale bar = 100 μm). Dashed white box indicates the band in layer 5 (L5) from which electrophysiological recordings were made. *Far right*, Confocal image of CT neurons (red) and CP neurons (green) and their co-localization in layer 5 (scale bar = 25 μm). (Representative images, n = 3 mice).

**B)** Summary of relative density of CC, CT, CP and dual-labeled neurons (CC + CT, or CP + CT) counted per slice (n = 9 slices from 3 mice for both CC / CT and CP / CT comparisons). CC and CT neurons represent distinct, non-overlapping populations of layer 5 pyramidal neurons, whereas CP and CT show partial overlap.

**C)** Sholl analysis of reconstructed dendrites from 2-photon images of CC (black) and CT (red) neurons (n = 6 CC neurons, n = 6 CT neurons) (n = 8 mice total).

**D)** Summary of total, basal and apical dendrite lengths of reconstructed dendrites of CC and CT neurons. CT neurons have more elaborate morphologies than CC neurons across multiple dendritic domains.

**E)** *Left*, Subcellular mapping of cPFC inputs onto different dendritic domains as specified by distances from the midline. *Right*, Average cPFC-evoked EPSCs at the soma (dark traces) and apical dendrites (light traces) of CC (*top*) (n = 7 neurons) and CT (*bottom*) (n = 7 neurons) neurons (n = 5 mice total), recorded in the presence of TTX and 4-AP. Arrows indicate light pulse.

**F)** Summary of cPFC-evoked EPSC amplitudes at different distances from the midline, normalized to the somatic response, from recordings in (E).

Values are mean ± SEM, * $p<0.05$.

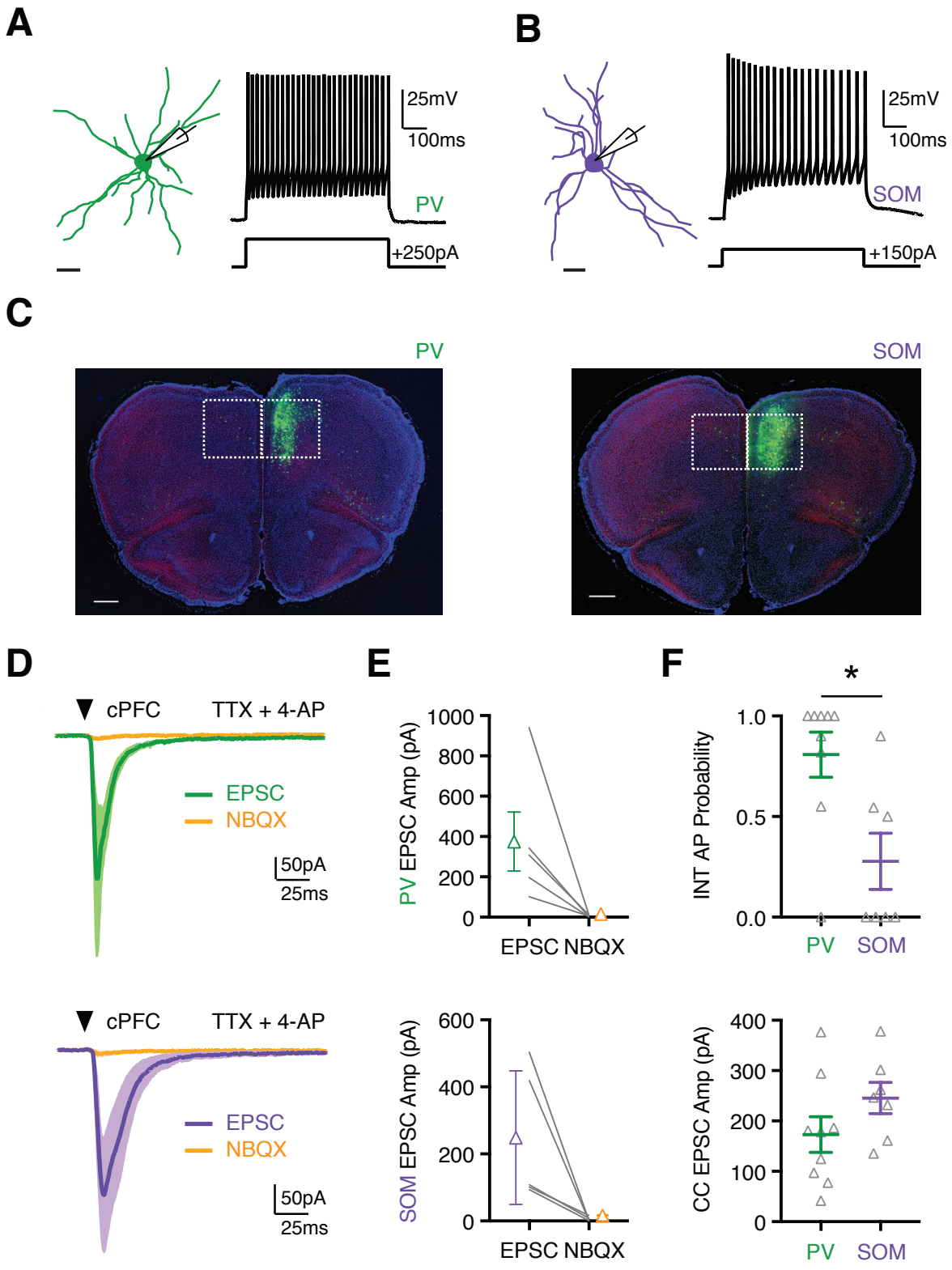


Anastasiades et al., Figure S2

**Figure S2: Callosal inputs contact both PV+ and SOM+ interneurons in PFC**

***Related to Figure 2.***

**A)** Dendritic reconstruction of 2-photon images (*left*) and current-clamp response (*right*) of PV+ interneuron, showing characteristic firing properties. Scale bar = 25 μm.

**B)** Same for SOM+ interneuron.

**C)** *Left*, Injection site and contralateral hemisphere of PV-Cre mouse after conditional rabies virus injection. *Right*, Similar but for a SOM-Cre mouse. Scale bars = 500 μm. Dashed boxes show regions enlarged in Fig. 2B. (Representative images, n = 3 mice).

**D)** *Top*, Average cPFC-evoked EPSCs at PV+ interneurons, recorded in the presence of TTX and 4-AP, and in the presence or absence of NBQX (n = 5 neurons, 4 mice). *Bottom*, Similar for SOM+ interneurons (n = 5 neurons, 3 mice). Arrow indicates light pulse (8 ms duration). Both PV+ and SOM+ interneurons receive monosynaptic glutamatergic input from the cPFC.

**E)** *Top*, Summary of cPFC-evoked EPSC amplitudes at PV+ interneurons, before and after bath application of NBQX. *Bottom*, Similar for SOM+ interneurons.

**F)** *Top,* Summary of AP probability for PV+ and SOM+ interneurons for light durations of 4 ms in the data shown in Fig. 2E & F. *Bottom,* Summary of cPFC-evoked EPSC amplitudes recorded from adjacent CC neurons for light durations of 4 ms in the data shown in Fig. 2E & F. PV+ neurons show greater firing probability, despite similar excitatory drive to the network.

Values are mean ± SEM, * $p<0.05$.

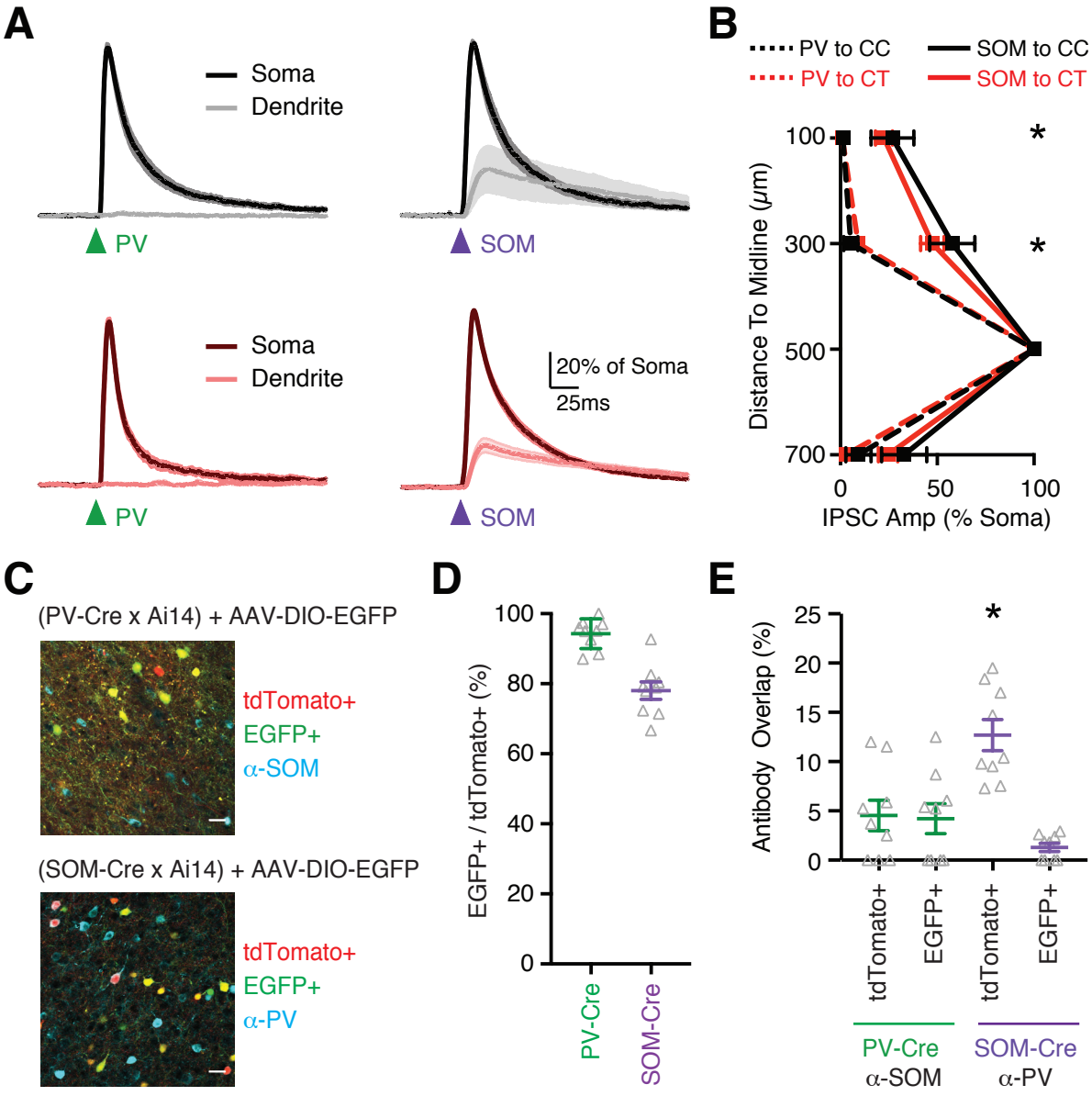


Anastasiades et al., Figure S3

**Figure S3: Anatomical specificity and subcellular targeting of inhibition**

***Related to Figure 3.***

**A)** *Left*, Average PV+-evoked IPSCs at the soma (dark traces) and apical dendrites (light traces) of CC neurons (*top*) (n = 7) and CT neurons (*bottom*) (n = 6) (n = 6 mice total), following schematic in Fig. S1. *Right,* Similar for SOM+-evoked IPSCs at CC neurons (n = 7) and CT neurons (n = 7) (n = 6 mice total).

**B)** Summary of IPSC amplitudes at different distances from the midline, normalized to the somatic response, from recordings in (A). PV+ inputs primarily target the soma, and SOM+ inputs also target the dendrites, but responses are similar in CC and CT neurons.

**C)** *Top*, Confocal images of layer 5 PFC, taken from PV-Cre x Ai14 mice that have been injected with AAV-FLEX-EGFP, showing tdTomato+ neurons due to Ai14 (red), EGFP+ neurons due to virus (green), and SOM+ antibody-stained neurons (cyan) (n = 9 slices from 3 mice). *Bottom*, Similar images for SOM-Cre x Ai14 mice, with PV+ antibody-stained neurons (cyan) (n = 9 slices from 3 mice). Scale bars = 25 μm.

**D)** Summary of percentage of tdTomato+ neurons that are also EGFP+ neurons, from experiments shown in (C). Viral infection labels a large proportion of PV+ and SOM+ interneurons that are labeled by the Ai14 reporter line. Labeling of fewer SOM+ interneurons is consistent with their known mislabeling by the Ai14 reporter line.

**E)** Summary of percentage of tdTomato+ or EGFP+ neurons that are co-labeled with antibodies for the opposing interneuron subtype in PV- or SOM-Cre x Ai14 mice. There is minimal labeling of PV+ interneurons by the SOM antibody using either viral or transgenic labeling. However, there is marked labeling of SOM+ interneurons by the PV antibody using the Ai14 reporter line, but not with the virus. This suggests that some PV+ interneurons will be targeted with the Ai14 reporter line, but not with our viral approaches.

Values are mean ± SEM, * $p<0.05$.

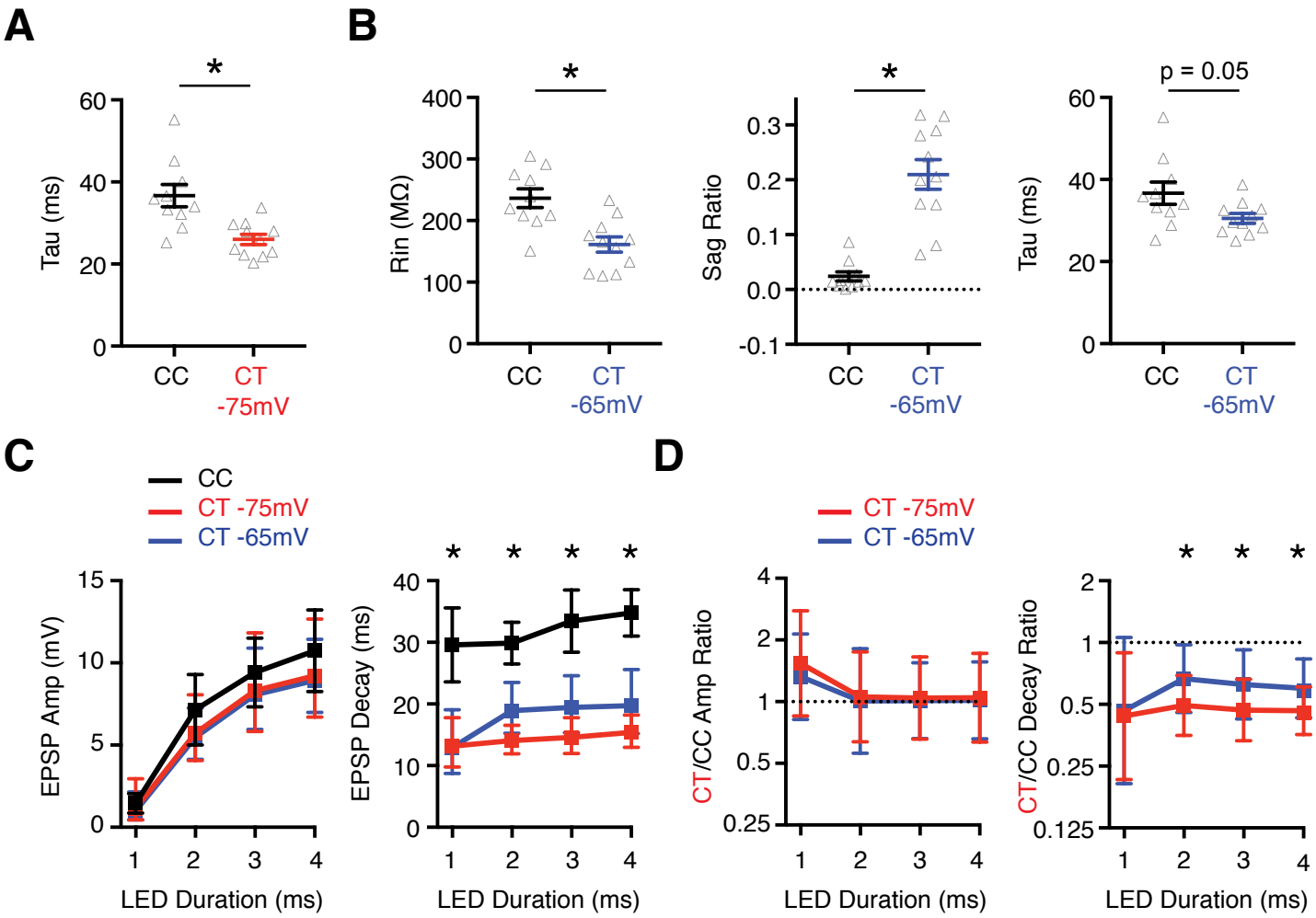


Anastasiades et al., Figure S4

**Figure S4: Distinct intrinsic and synaptic responses at CC and CT neurons**

***Related to Figure 4.***

**A)** Summary of membrane time constant (Tau) of CC and CT neurons recorded at -75 mV, showing faster intrinsic kinetics at CT neurons.

**B)** Summary of input resistance ($R_{in}$), voltage sag in response to hyperpolarization (Sag Ratio), and membrane time constant (Tau) for cells shown in Fig. 4C, with CC neurons held at -75 mV and CT neurons held at -65 mV, indicating qualitatively similar differences to the same CT neurons at -75 mV shown in Fig. 4C.

**C)** Summary of cPFC-evoked EPSP amplitudes (*left*) and decays (*right*) across a range of light durations (from data shown in Fig. 4 D - E), with CC neurons held at -75 mV and CT neurons held at both -75mV and -65mV. Faster EPSP decay is present in CT neurons at both potentials (n = 8 pairs, 6 mice).

**D)** Summary of CT / CC amplitude (*left*) and decay (*right*) ratios, with y-axis on log2 scale.

Values are mean ± SEM (A-C) or geometric mean ± CI (D), * $p<0.05$.

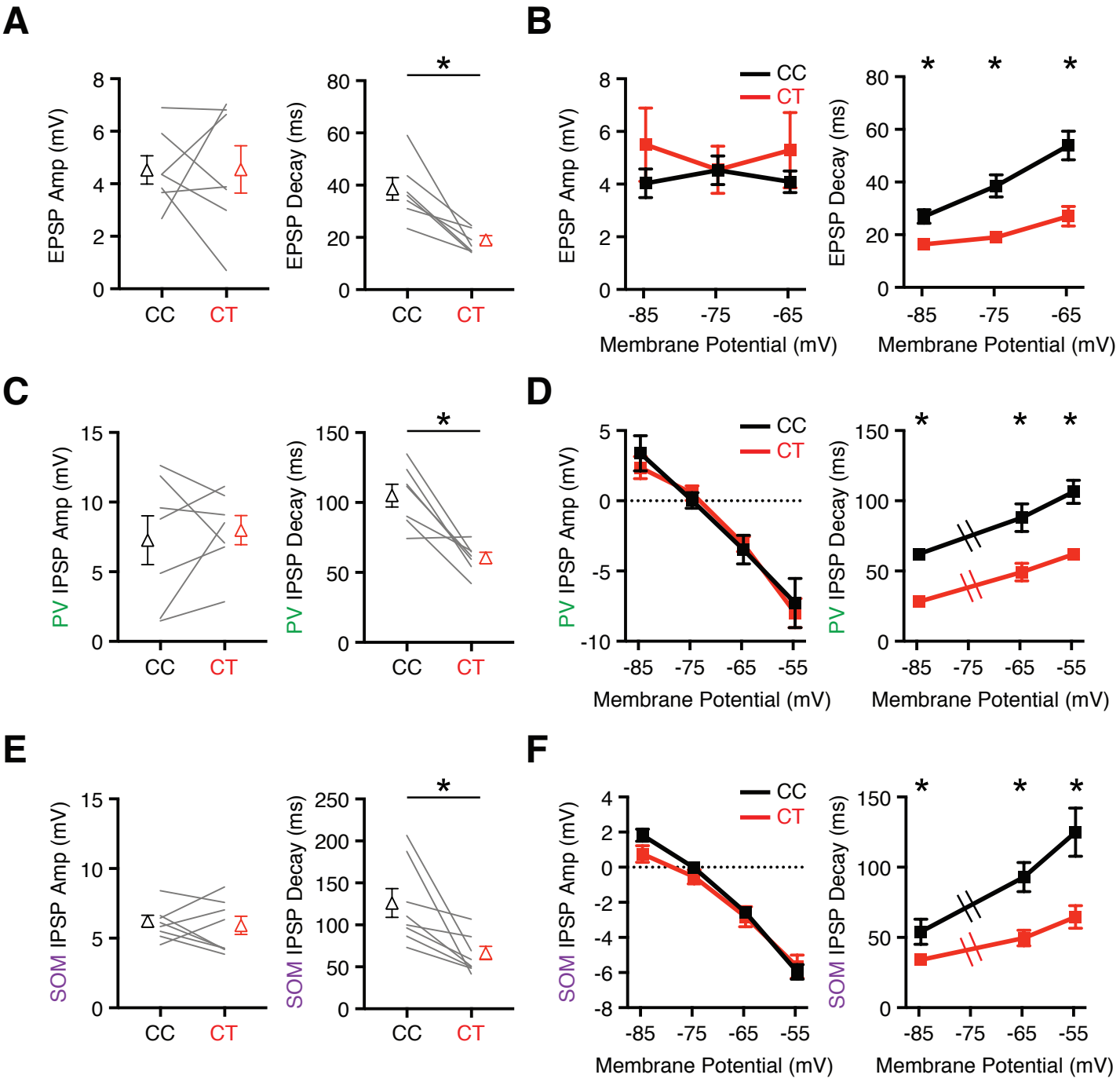


Anastasiades et al., Figure S5

**Figure S5: Properties of EPSPs and IPSPs depend on membrane potential**

***Related to Figure 5.***

**A)** Summary of cPFC-evoked EPSP amplitudes (*left*) and decays (*right*) for pairs of CC and CT neurons recorded at -75 mV (n = 7 pairs, as shown in Fig. 5A).

**B)** Summary of cPFC-evoked EPSP amplitudes (*left*) and decays (*right*) recorded across multiple membrane potentials at pairs of CC and CT neurons. EPSP amplitudes are similar at these cell types across a range of membrane potentials but decays remain distinct. Data is displayed from the same neurons recorded at each potential.

**C)** Similar to (A) for PV+ IPSPs recorded at -55 mV (n = 7 pairs, as shown in Fig. 5B).

**D)** Similar to (B) for PV+ IPSPs. IPSP amplitudes are similar at these cell types across a range of membrane potentials but decays remain distinct.

**E)** Similar to (A) for SOM+ IPSPs recorded at -55 mV (n = 8 pairs, as shown in Fig. 5B).

**F)** Similar to (D) for SOM+ IPSPs. IPSP amplitudes are similar at these cell types across a range of membrane potentials but decays remain distinct.

Note that IPSP decay is not reported at -75 mV due to its proximity to $E_{Cl}$.

Values are mean ± SEM, * $p<0.05$.

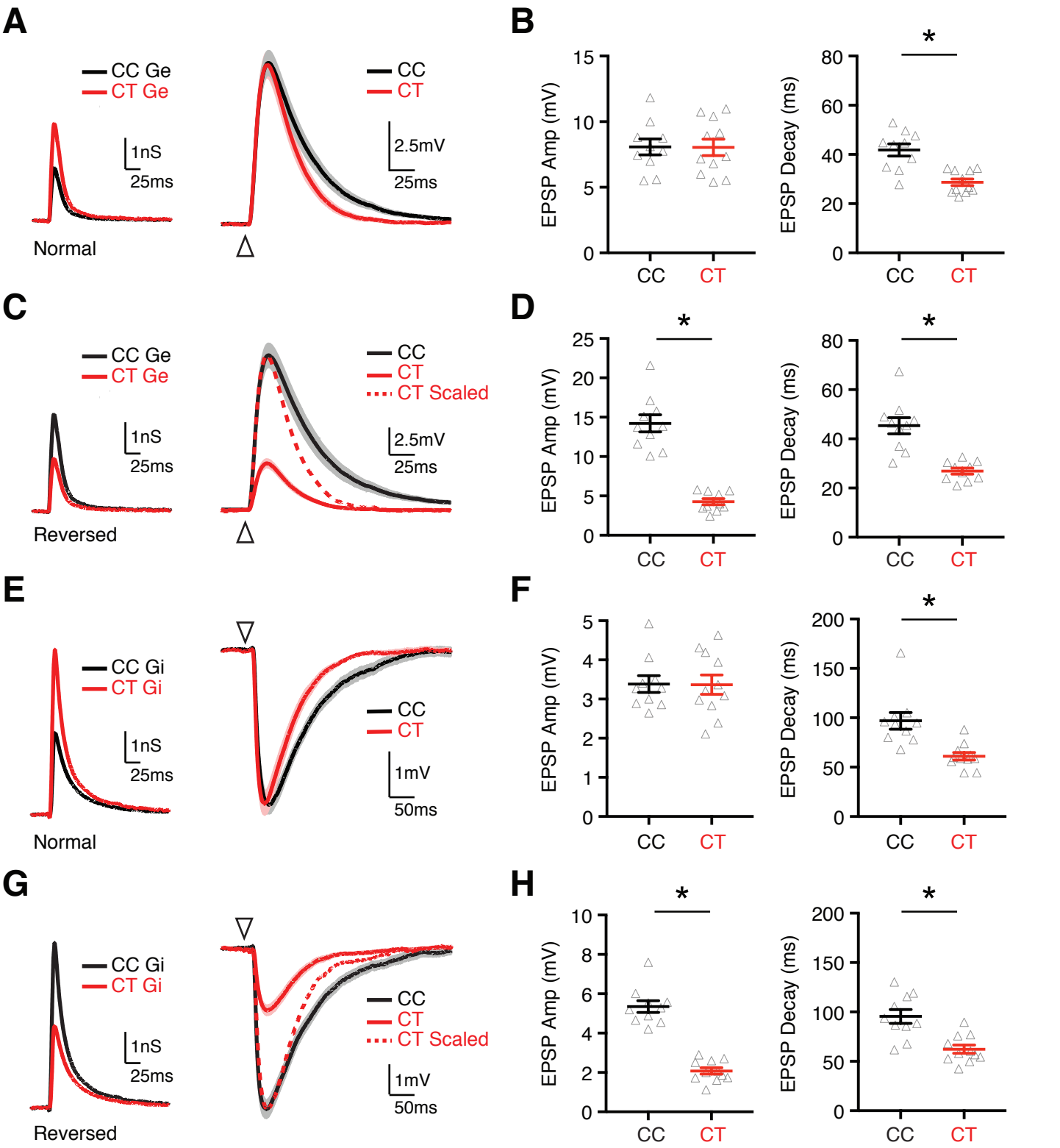


Anastasiades et al., Figure S6

**Figure S6: EPSPs and IPSPs reflect both targeting and intrinsic properties**

***Related to Figure 7.***

**A)** *Left*, Excitatory conductance waveforms injected into CC (black) (n = 10 neurons) and CT (red) (n = 11 neurons) (n = 6 mice total) neurons in dynamic-clamp recordings, derived from EPSCs measured in Fig. 1F. *Right*, Average conductance-evoked EPSPs recorded in dynamic-clamp at -75 mV from CC and CT neurons. Arrows indicate conductance onset.

**B)** Summary of EPSP amplitude (*left*) and decay (*right*) for recordings in (A). Amplitudes are similar at the two cell types, but decays are much faster at CT neurons.

**C)** Similar recordings to (A), where the normal conductances have now been reversed, such that CC neurons (black) receive the larger conductance, and CT neurons (red) receive the smaller. Dashed red line shows CT EPSP scaled to the peak of CC EPSP, highlighting the persistent difference in EPSP decay. Arrows indicate conductance onset.

**D)** Summary of EPSP amplitude (*left*) and decay (*right*) for recordings in (C). Amplitudes are now much larger at CC neurons, but decays remain much faster at CT neurons.

**E – H)** Similar to (A - D) for inhibitory conductances derived from IPSCs measured in Fig. 1E and conductance-evoked IPSPs recorded at -55 mV in the same CC and CT neurons as in (A). For normal targeting, amplitudes are similar at the two cell types, but decays are much faster at CT neurons. For reversed targeting, amplitudes are now much larger at CC neurons, but decays are still faster at CT neurons. Together, these data highlight the importance of both targeting of synaptic inputs and intrinsic properties of postsynaptic cells.

Values are mean ± SEM, * $p<0.05$.

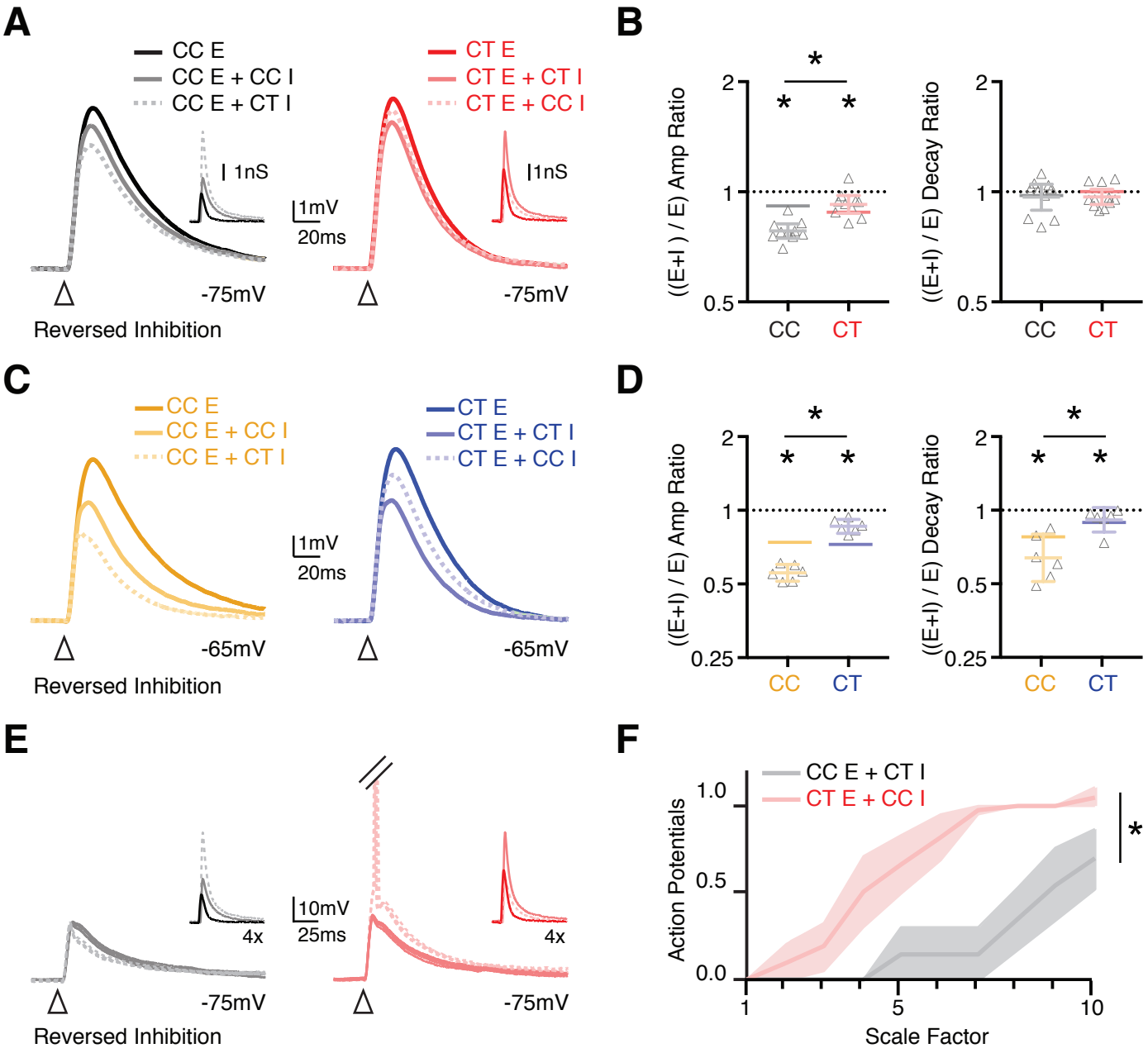


Anastasiades et al., Figure S7

**Figure S7: Reversing inhibitory targeting unbalances EPSPs and evoked firing**

***Related to Figure 7.***

**A)** Average conductance-evoked EPSPs recorded in dynamic-clamp at -75 mV from CC (*left*) and CT (*right*) neurons (as shown in Fig. 7A - B). EPSPs are evoked by cell-type appropriate excitation alone (black and red traces), or paired with either cell-type appropriate inhibition (grey and pink traces), or paired with reversed inhibition in which CC neurons receive CT inhibition and vice versa (dashed grey and pink traces). Arrows indicate conductance onset. Inset traces show injected conductances.

**B)** Summary of ((E + I) / E) amplitude (*left*) and decay (*right*) ratios for recordings in (A). Solid grey and pink bars indicate average values derived from cell-type appropriate inhibition, as shown in Fig. 7B. Reversing inhibition significantly increases the suppression of CC neurons and reduce that of CT neurons. y-axis is on log2 scale.

**C – D)** Similar to (A - B) for dynamic-clamp recordings at -65 mV. Reversing inhibition again leads to greater suppression of CC (n = 6) than CT (n = 6) neurons (n = 3 mice total). Moreover, reversing inhibition now preferentially accelerates the decay at CC over CT neurons.

**E)** Conductance-evoked EPSPs and action potentials recorded in dynamic-clamp at -75 mV from CC (*left*) (n = 8) and CT (*right*) (n = 8) neurons (as shown in Fig. 7C - E), showing response to cell-type appropriate (darker grey and pink traces) or reversed inhibition (dashed grey and pink traces). Traces are truncated to highlight subthreshold responses. Inset traces show injected conductances with 4x scale factor.

**F)** Summary of number of action potentials evoked at CC and CT neurons in response to different scale factors of cell-type appropriate excitation paired with reversed inhibition. Reversing inhibition increases the suppression of CC neurons, and unbalances firing at the two cell types.

Values are geometric mean ± CI (B, D) or mean ± SEM (F), * $p<0.05$.